

The Basics of MEMS IMU/Gyroscope Alignment

By Mark Looney

Introduction

Sensor misalignment is often a key consideration for high performance motion control systems that use MEMS inertial measurement units (IMUs) in their feedback loops. For the gyroscopes in the IMU, sensor misalignment describes the angular difference between each gyroscope's axis of rotation and the system defined *inertial reference frame*, also known as the *global frame*. Managing the impact that misalignment has on sensor accuracy can require unique packaging, special assembly processes, or even complex inertial testing in the final configuration. All of these things can have a major impact on important project management metrics such as schedule, investment, and the total cost associated with the IMU in each system. Therefore, sensor alignment is a metric that warrants consideration during early stages of the design cycle, while there is time to define the system architecture around the most efficient solution. After all, nobody wants to burn through 80% of their project schedule and budget to find out that their inexpensive sensor requires hundreds, maybe even thousands, of dollars in unexpected cost adders to meet nonnegotiable deliverables to their end users. Ouch!

There are three basic alignment concepts to understand and evaluate when architecting an IMU function for a system: error estimation, understanding misalignment impact on key system behaviors, and electronic alignment (after installation). Initial error estimation should include error contributions from both the IMU and the mechanical system that holds it in place during operation. Understanding the impact that these errors have on a system's key functions helps establish relevant performance goals that prevent overworking the problem, while at the same time managing the risk of missing key performance and cost commitments. Finally, some form of electronic alignment might be necessary for optimizing a system's performance/cost trade space.

Predicting Alignment Error After Installation

The alignment accuracy in an application will depend on two key things: the IMU's misalignment error and the precision of the mechanical system that holds it in place during operation. The IMU's contribution (Ψ_{IMU}) and the system's contribution (Ψ_{SYS}) are not typically related to each other, so estimating the total misalignment error often comes from combining these two error sources using a root-sum-square calculation:

$$\Psi_T = \sqrt{\Psi_{\text{IMU}}^2 + \Psi_{\text{SYS}}^2} \quad (1)$$

Some IMU specification tables quantify misalignment errors through parameters such as *axis to package misalignment error* or *axis to frame misalignment error*. Figure 1 provides an exaggerated view of these misalignment errors for each gyroscope in the ADIS16485, with respect to the edges of its package. In this illustration, the green, dashed lines represent the axes in the package defined reference frame. The solid lines represent the axes of rotation for the gyroscopes inside of the package and Ψ_{IMU} represents the maximum of the three misalignment terms (Ψ_x, Ψ_y, Ψ_z).

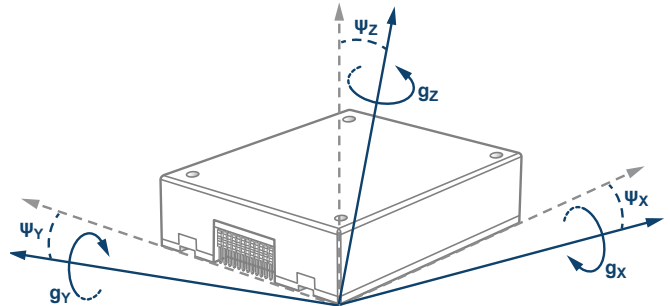


Figure 1. ADIS16485 axis to frame misalignment.

Predicting the system's contribution (Ψ_{SYS} in Equation 1) to misalignment error involves analyzing any opportunity for mechanical imperfection that can skew the IMU's resting place in the system, with respect to the global frame. When using an IMU that solders to a printed circuit board, this will involve consideration of things like original placement accuracy, variation in solder deposition, float during solder reflow, tolerances of key PCB features (like mounting holes), and tolerances of the system frame itself. When using a module level IMU, more direct coupling to the system enclosure may be possible, as shown in Figure 2. This type of interface has two key mechanical features, that help manage the mounting skew errors, the mounting ledges (4x), and the mounting nest.

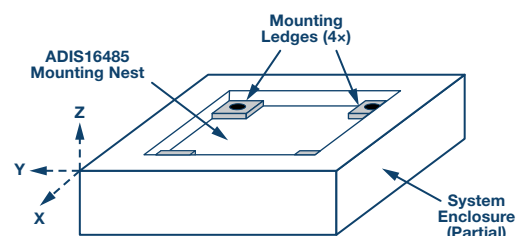


Figure 2. Nested baseplate design concept.

In this type of mounting scheme, variation in the height of the four mounting ledges is one example of mechanical variation that can cause mounting skew in the x-axis and y-axis. Figure 3 provides an exaggerated illustration to help explain the impact that this variation (H1 vs. H2) has on the mounting skew (Ψ_x), with respect to the x-axis.

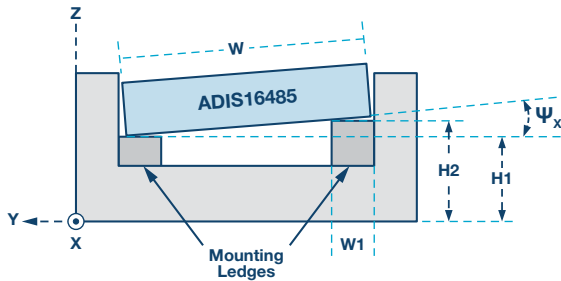


Figure 3. Misalignment error due to mounting ledge variation.

Equation 2 provides a relationship for predicting the x-axis skew angle (Ψ_x) associated with the difference in height (H2 to H1) and the span between the two points of contact (W to W1):

$$\Psi_x = \arctan\left(\frac{H2 - H1}{W - W1}\right) \text{ when } H2 - H1 \ll W - W1 \quad (2)$$

The variation in mounting ledge height will have a similar impact on mounting skew around the y-axis. In that case, substitute the package length (L) for the width (W) in Equation 2 to develop the following relationship for estimating y-axis skew angle (Ψ_y):

$$\Psi_y = \arctan\left(\frac{H2 - H1}{L - W1}\right) \text{ when } H2 - H1 \ll L - W1 \quad (3)$$

Figure 4 provides another example of how a mechanical attribute can impact mounting skew around the z-axis. In this case, machine screws will slide through mounting holes in the IMU body (in all four corners), through holes in the mounting ledge, and then into locking nuts on the backside of the mounting ledges. In this scenario, the difference between the diameter of the machine screws (D_M) and their associated pass-through holes (D_H) in the baseplate present an opportunity for skew in the z-axis.

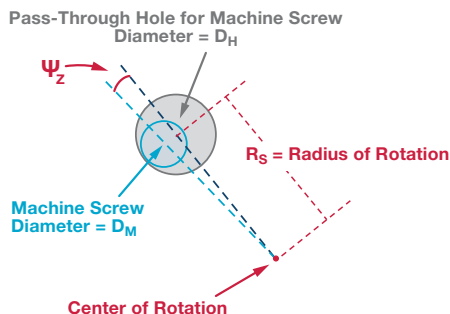


Figure 4. Mounting screw/hole impact on z-axis skew angle.

Equation 4 provides a relationship for predicting the opportunity for z-axis mounting skew (Ψ_z), based on this difference in diameters and the radius of rotation (R_S), which is equal to one half of the distance between the two mounting screws in opposite corners.

$$\Psi_z = 2 \times a \tan\left(\frac{D_H - D_M/2}{2 \times R_S}\right) \quad (4)$$

Example 1

Estimate the overall misalignment associated with using 2 mm machine screws to mount the ADIS16485 onto 6 mm \times 6 mm mounting ledges, which have 2.85 mm holes and a height tolerance of 0.2 mm.

Solution

Using the nominal width (W) of 44 mm, the x-axis skew angle (see Figure 3) prediction is 0.3°.

$$\Psi_x = \arctan\left(\frac{H2 - H1}{W - W1}\right) = \arctan\left(\frac{0.2 \text{ mm}}{44 \text{ mm} - 6 \text{ mm}}\right) = 0.3^\circ$$

The nominal distances between the mounting holes on each side of this package are 39.6 mm and 42.6 mm, respectively. These dimensions form the two sides of a right angle triangle, whose hypotenuse is equal to the distance between the two holes in opposite corners of the package. The radius of the rotation (R_S , see Figure 4) is equal to one half of this distance (29.1 mm), which leads to a prediction of 0.83° of skew in the z-axis.

$$R_S = \frac{\sqrt{39.6^2 + 42.6^2}}{2} \approx 29.1 \text{ mm}$$

$$\Psi_z = 2 \times a \tan\left(\frac{D_H - D_M/2}{2 \times R_S}\right) = 2 \times a \tan\left(\frac{2.85 - 2/2}{2 \times 29.1}\right) \approx 0.83^\circ$$

For the composite prediction formula in Equation 1, Ψ_{SYS} is equal to Ψ_z (maximum from estimates) and Ψ_{IMU} is equal to 1°, per the axis to frame misalignment error specification in the IMU's data sheet. This generates a total misalignment error estimate of 1.28°.

$$\Psi_T = \sqrt{\Psi_{\text{IMU}}^2 + \Psi_{\text{SYS}}^2} = \sqrt{1^2 + 0.8^2} = \sqrt{1.64} = 1.28^\circ$$

Misalignment Impact on System Accuracy

Understanding the basic relationship between misalignment errors and the impact that they have on gyroscope accuracy is a good place to start when developing accuracy criteria

for an application. To start this process, Figure 5 provides a generic illustration of a three axis gyroscope system. In this diagram, the three solid green lines represent the three axes in the global frame, the black solid lines represent the axes of rotation for all three gyroscopes, and the Ψ -based labels represent the misalignment errors between global frame and gyroscope axes. Equation 5, Equation 6, and Equation 7 demonstrate the impact that the misalignment errors have on each gyroscope's response to rotation around its assigned axis in the global frame. In these equations, the cosine of the misalignment angle introduces a scale error.

$$G_X = \omega_X \times \cos(\Psi_X) \quad (5)$$

$$G_Y = \omega_Y \times \cos(\Psi_Y) \quad (6)$$

$$G_Z = \omega_Z \times \cos(\Psi_Z) \quad (7)$$

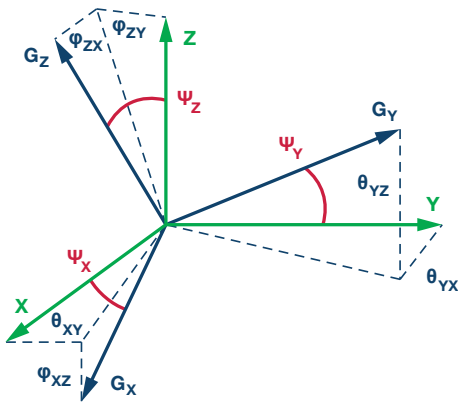


Figure 5. Orthogonal three axis gyroscopes with alignment errors.

Misalignment errors also introduce cross-axis influences on each axis. Quantifying these influences requires breaking the misalignment angle for each axis down into two components, which relate to the two other axes. For example, Ψ_X has a y-axis component (ϕ_{XY}) and a z-axis component (ϕ_{XZ}), which results in the following expansion of the x-axis gyroscope response to rotation around all three axes in the global frame ($\omega_X, \omega_Y, \omega_Z$):

$$G_X = \omega_X \times \cos(\Psi_X) + \omega_Y \times \sin(\phi_{XY}) + \omega_Z \times \sin(\phi_{XZ}) \quad (8)$$

This same expansion applies to the y-axis and z-axis gyroscopes:

$$G_Y = \omega_X \times \sin(\phi_{YX}) + \omega_Y \times \cos(\Psi_Y) + \omega_Z \times \sin(\phi_{YZ}) \quad (9)$$

$$G_Z = \omega_X \times \sin(\phi_{ZX}) + \omega_Y \times \sin(\phi_{ZY}) + \omega_Z \times \cos(\Psi_Z) \quad (10)$$

Integrating both sides of Equation 8, Equation 9, and Equation 10 produces similar relationships, which are in terms of angle displacement. In the resulting Equation 11, Equation 12, and Equation 13, the angles of interest are the angular displacement around the global frame ($\theta_{X\omega}, \theta_{Y\omega}, \theta_{Z\omega}$) and the integration of each gyroscope ($\theta_{XG}, \theta_{YG}, \theta_{ZG}$).

$$\theta_{XG} = \theta_{X\omega} \times \cos(\Psi_X) + \theta_{Y\omega} \times \sin(\phi_{XY}) + \theta_{Z\omega} \times \sin(\phi_{XZ}) \quad (11)$$

$$\theta_{YG} = \theta_{X\omega} \times \sin(\phi_{YX}) + \theta_{Y\omega} \times \cos(\Psi_Y) + \theta_{Z\omega} \times \sin(\phi_{YZ}) \quad (12)$$

$$\theta_{ZG} = \theta_{X\omega} \times \sin(\phi_{ZX}) + \theta_{Y\omega} \times \sin(\phi_{ZY}) + \theta_{Z\omega} \times \cos(\Psi_Z) \quad (13)$$

Example 2

A ground-based, unmanned vehicle (UV) is using a MEMS IMU as a feedback sensor in a platform stabilization control (PSC) system for its antenna. This system employs an RSS tuner loop that requires the azimuth and elevation angles to stay within $\pm 1^\circ$ to maintain continuous communication. During the most dynamic conditions, the PSC relies heavily on the y-axis gyroscope's measurement for elevation angle control and the z-axis gyroscope's measurements for azimuth angle control. The maximum change in heading ($\theta_{Z\omega}$) during these dynamic conditions is 30° and there is no rotation around the x-axis or y-axis ($\theta_{X\omega} = \theta_{Y\omega} = 0$) during this maneuver.

Solution

Zero rotation around the x-axis and y-axis enable Equation 8 and Equation 9 to reduce to the following:

$$\begin{aligned} \theta_{YG} &= \theta_{Z\omega} \times \sin(\phi_{YZ}) \\ \theta_{ZG} &= \theta_{Z\omega} \times \cos(\Psi_Z) \end{aligned}$$

Starting with the y-axis, establish a maximum boundary of 1° for θ_{YG} and solve for the misalignment term Φ_{YZ} . This process establishes a maximum allowable misalignment error of 1.9° for the y-axis gyroscope.

$$\begin{aligned} \phi_{YZ} &\leq \sin^{-1}\left(\frac{\theta_{YG}}{\theta_{Z\omega}}\right) \\ \phi_{YZ} &\leq \sin^{-1}\left(\frac{1^\circ}{30^\circ}\right) \\ \phi_{YZ} &\leq 1.9^\circ \end{aligned}$$

For the z-axis, set $\theta_{Z\omega}$ equal to 30° and establish a maximum boundary of 1° for the difference between θ_{ZG} and $\theta_{Z\omega}$, then solve for Ψ_Z . This process establishes a maximum allowable misalignment error of 14.8° on the z-axis gyroscope.

$$\begin{aligned} \theta_{Z\omega} - \theta_{ZG} &\leq 1^\circ \\ \theta_{Z\omega} - \theta_{Z\omega} \times \cos(\Psi_Z) &\leq 1^\circ \\ \theta_{Z\omega} - 1^\circ &\leq \theta_{Z\omega} \times \cos(\Psi_Z) \\ 1 - \frac{1^\circ}{\theta_{Z\omega}} &\leq \cos(\Psi_Z) \\ \Psi_Z &\leq \cos^{-1}\left[1 - \frac{1^\circ}{\theta_{Z\omega}}\right] \\ \Psi_Z &\leq \cos^{-1}\left[1 - \frac{1^\circ}{30^\circ}\right] \\ \Psi_Z &\leq 14.8^\circ \end{aligned}$$

These calculations reveal that the cross-axis behaviors between the y-axis and z-axis will drive the alignment accuracy requirement of $\sim 1.9^\circ$, for this specific maneuver/scenario.

Electronic Alignment

In cases where an IMU and attachment system will not meet critical system objectives, electronic alignment provides a method for reducing the misalignment errors. This process has two key steps: characterize the misalignment terms (after IMU installation) and develop a correcting alignment matrix that corrects the gyroscopes to respond as if they were aligned with the global frame, when it's applied to the gyroscope

array. Equation 14 provides a system model for this process, where rotation around each axis in the global frame ($\bar{\omega}$) are the three system inputs, the three gyroscope responses (\bar{G}) are the system outputs, and a 3×3 matrix (M) represents the system behaviors (including misalignment) between the inputs and outputs.

$$\bar{G} = M \times \bar{\omega} \quad (14)$$

Simple algebraic manipulation determines that product of the gyroscope measurements (\bar{G}) and inverse of M (M^{-1}) is equal to the global frame's rotation array ($\bar{\omega}$). Therefore, the alignment matrix is equal to M^{-1} .

$$\begin{aligned} M^{-1} \times \bar{G} &= M^{-1} \times M \times \bar{\omega} \\ M^{-1} \times \bar{G} &= \bar{\omega} \end{aligned} \quad (15)$$

Equation 8, Equation 9, and Equation 10 provide the basis for expanding equation 14 to include the misalignment terms in Equation 16 and more generically in Equation 17 and Equation 18:

$$\begin{bmatrix} G_X \\ G_Y \\ G_Z \end{bmatrix} = \begin{bmatrix} \cos(\Psi_X) & \sin(\phi_{XY}) & \sin(\phi_{XZ}) \\ \sin(\phi_{YX}) & \cos(\Psi_Y) & \sin(\phi_{YZ}) \\ \sin(\phi_{ZX}) & \sin(\phi_{ZY}) & \cos(\Psi_Z) \end{bmatrix} \begin{bmatrix} \omega_X \\ \omega_Y \\ \omega_Z \end{bmatrix} \quad (16)$$

$$\begin{bmatrix} G_X \\ G_Y \\ G_Z \end{bmatrix} = \begin{bmatrix} M_{11} & M_{12} & M_{13} \\ M_{21} & M_{22} & M_{23} \\ M_{31} & M_{32} & M_{33} \end{bmatrix} \begin{bmatrix} \omega_X \\ \omega_Y \\ \omega_Z \end{bmatrix} \quad (17)$$

$$M = \begin{bmatrix} M_{11} & M_{12} & M_{13} \\ M_{21} & M_{22} & M_{23} \\ M_{31} & M_{32} & M_{33} \end{bmatrix} \quad (18)$$

Rotating the entire system around one axis at a time simplifies the system model enough to isolate each element in the matrix to one of the gyroscope measurements. For example, rotating the system around the x-axis ($\omega_X = \omega_{TR}$, $\omega_Y = 0$, $\omega_Z = 0$) while observing all three gyroscopes helps simplify the relationships for M11, M21, and M31 to the following:

$$M_{11} = \frac{G_X}{\omega_{TR}} \quad (19)$$

$$M_{21} = \frac{G_Y}{\omega_{TR}} \quad (20)$$

$$M_{31} = \frac{G_Z}{\omega_{TR}} \quad (21)$$

Using the same approach, y-axis rotation ($\omega_X = 0$, $\omega_Y = \omega_{TR}$, $\omega_Z = 0$) helps simplify the relationships for M12, M22, and M32 to the following:

$$M_{12} = \frac{G_X}{\omega_{TR}} \quad (22)$$

$$M_{22} = \frac{G_Y}{\omega_{TR}} \quad (23)$$

$$M_{32} = \frac{G_Z}{\omega_{TR}} \quad (24)$$

Finally, z-axis rotation ($\omega_X = 0$, $\omega_Y = 0$, $\omega_Z = \omega_{TR}$) helps simplify the relationships for M13, M23, and M33 to the following:

$$M_{13} = \frac{G_X}{\omega_{TR}} \quad (25)$$

$$M_{23} = \frac{G_Y}{\omega_{TR}} \quad (26)$$

$$M_{33} = \frac{G_Z}{\omega_{TR}} \quad (27)$$

Obviously, the accuracy of the motion profile ($\bar{\omega}$) and gyroscope measurements (\bar{G}) have a direct impact on this process. In particular, off-axis motion can have a significant impact on this process, so it should be a strong consideration when purchasing and deploying inertial test equipment that will execute on these requirements. With respect to the gyroscope accuracy, bias and noise are two threats to accuracy that typically require consideration during this process. One technique for managing the impact of residual bias error (b_E) in the gyroscope measurements is through using two different rates of rotation, which are equal and opposite to each other. For example, when rotating in the positive direction around the y-axis ($\omega_Y = \omega_{TR}$, $\omega_X = \omega_Z = 0$), Equation 28 describes the z-axis gyroscope response, with bias error. Equation 29 describes the z-axis gyroscope response when rotating around the y-axis in the negative direction ($\omega_Y = -\omega_{TR}$, $\omega_X = \omega_Z = 0$):

$$G_{ZP} = M_{32} \times \omega_{TR} + b_E \quad (28)$$

$$G_{ZN} = -M_{32} \times \omega_{TR} + b_E \quad (29)$$

Rearrange Equation 29 to relate to the bias error (b_E), substitute it into Equation 28, and then solve for M32. Notice how the bias error (b_E) drops out of the formula.

$$G_{ZN} = -M_{32} \times \omega_{TR} + b_E$$

$$b_E = G_{ZN} + M_{32} \times \omega_{TR}$$

$$G_{ZP} = M_{32} \times \omega_{TR} + G_{ZN} + M_{32} \times \omega_{TR}$$

$$G_{ZP} - G_{ZN} = M_{32} \times \omega_{TR} + M_{32} \times \omega_{TR}$$

$$G_{ZP} - G_{ZN} = 2 \times M_{32} \times \omega_{TR}$$

$$M_{32} = \frac{G_{ZP} - G_{ZN}}{2 \times \omega_{TR}} = \frac{G_{ZP} - G_{ZN}}{(\omega_{ZP} - \omega_{ZN})} \quad (30)$$

This formula assumes that the bias error is constant during both measurements, which is not a realistic expectation, so it is wise to understand the opportunity for variation (temperature, time, and noise) from measurement to measurement.

When the measurements are taken in succession, under stable temperature conditions, noise is often the key error to manage in this process. The acceptable level of noise in the gyroscope measurements will depend on the alignment accuracy goal (Ψ_T) and the rate of rotation on each axis during the characterization (ω_{TR}). A common technique for noise reduction is through averaging a time record of gyroscope data, while the inertial conditions are constant. The Allan variance curves provides a tool for understanding the trade-off between repeatability (noise) and the averaging time.

Example 3

If the rate of rotation during characterization is $100^\circ/\text{s}$, the alignment accuracy goal is 0.1° , and the noise (rms) must be $10\times$ less than the misalignment goal, how long do we need to average the outputs of the ADIS16485 to achieve these objectives?

Solution

Using a generic response between a gyroscope and input (rotation on test platform), the following calculations reveal that the total noise (rms) in each gyroscope must be less than $62^\circ/\text{hour}$.

$$G_{\text{Noise}} \leq \frac{1}{10} \times \omega_{\text{TR}} \times \sin(\Psi_T)$$

$$G_{\text{Noise}} \leq 0.1 \times 100 \frac{\circ}{\text{s}} \times \sin(0.1^\circ)$$

$$G_{\text{Noise}} \leq 0.017 \frac{\circ}{\text{s}} = \sim 62 \frac{\circ}{\text{hour}}$$

Figure 6 provides an example of how to use the Allan variance curve for this IMU to select an averaging time to meet this requirement. In this case, an averaging time of 0.1 seconds meets the $62^\circ/\text{hour}$ objective for repeatability, with some margin.

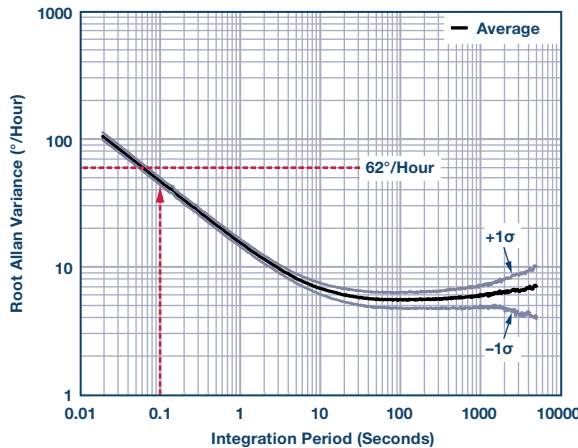


Figure 6. ADIS16485 Allan variance curve.

Note that this approach only accounts for the noise in the sensor itself. If the test platform has vibration that adds noise to the gyroscope measurements, that may require additional consideration and filtering.

Tips and Tricks for Simplifying the Process

Developing a triaxial inertial test system with the necessary precision and environmental control temperature typically requires a substantial investment in capital equipment and engineering development resources. For those who are developing first or second generation systems that have many questions to answer during development, these types of resources or time may not be available. This situation creates a need for a simpler solution, which can come through careful IMU selection and leveraging natural motion that is available in the instrument or in the application.

For example, sometimes working with angles may be more convenient than working with angular rate measurements. Equation 31 combines Equation 11, Equation 12, and Equation 13 to represent system behaviors (M) in terms of angles around the global frame ($\theta_{X\omega}, \theta_{Y\omega}, \theta_{Z\omega}$) and from integrating the gyroscope outputs ($\theta_{XG}, \theta_{YG}, \theta_{ZG}$):

$$\begin{bmatrix} \theta_{XG} \\ \theta_{YG} \\ \theta_{ZG} \end{bmatrix} = \begin{bmatrix} M_{11} & M_{12} & M_{13} \\ M_{21} & M_{22} & M_{23} \\ M_{31} & M_{32} & M_{33} \end{bmatrix} \begin{bmatrix} \theta_{X\omega} \\ \theta_{Y\omega} \\ \theta_{Z\omega} \end{bmatrix} \quad (31)$$

With respect to device selection, axis to axis misalignment error is a key parameter to consider, because when it is lower than the axis to package misalignment parameter, it can help reduce the complexity of the inertial test profile (in Equation 16) associated with electronic alignment. While the axis to package misalignment parameter describes gyroscope orientation, with respect to an external mechanical reference, the axis to axis misalignment parameter relates the orientation of each gyroscope with respect to the other two gyroscopes. Most often, the ideal orientation for the three gyroscopes in a MEMS IMU is 90° from each other, so axis to axis misalignment relates to another common parameter for this behavior—cross-axis sensitivity. Using Figure 7 as a reference, axis to axis misalignment would represent the maximum of these three relationships:

$$\phi_{xye} = \phi_{xy} - 90^\circ \quad (32)$$

$$\phi_{yze} = \phi_{yz} - 90^\circ \quad (33)$$

$$\phi_{zxe} = \phi_{zx} - 90^\circ \quad (34)$$

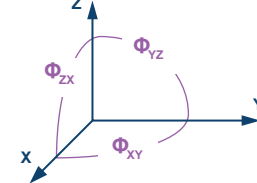


Figure 7. Axis to axis misalignment diagram.

The axis to axis misalignment parameter establishes the error associated with assuming that the sensors have perfect orthogonal alignment when developing an electronic alignment process. Using the perfectly orthogonal assumption, one can align all three axes through only two axes of rotation. For example, rotating around the y-axis and z-axis provides for direct observation of $M_{12}, M_{13}, M_{22}, M_{23}, M_{32}$, and M_{33} . Assuming perfect orthogonal alignment and applying some trigonometric properties enables calculation of the other three elements (M_{11}, M_{21} , and M_{31}) using the six elements and the following relationships:

$$M_{21} = M_{12} \quad (35)$$

$$M_{31} = M_{13} \quad (36)$$

$$M_{11} = \sqrt{1 - M_{12}^2 - M_{13}^2} \quad (37)$$

These identities result in the following update to the system model, where all nine elements in the M matrix are in terms of the six elements that come from y-axis and z-axis rotation.

$$\begin{bmatrix} G_X \\ G_Y \\ G_Z \end{bmatrix} = \begin{bmatrix} \sqrt{1 - M_{12}^2 - M_{13}^2} & M_{12} & M_{13} \\ M_{12} & M_{22} & M_{23} \\ M_{13} & M_{23} & M_{33} \end{bmatrix} \begin{bmatrix} \omega_X \\ \omega_Y \\ \omega_Z \end{bmatrix} \quad (38)$$

Conclusion

Inertial MEMS technology has made amazing advances in the past few years, providing system developers with a wide range of options inside a complex trade space that includes size, weight, power, unit cost, integration cost, and performance. For those who are architecting motion control systems with MEMS IMU for the first time, there are a lot of things to learn, with respect to selecting the right IMU and preparing

to support critical system requirements with this IMU. Since alignment accuracy can have a significant impact on critical performance, cost, and schedule objectives, it is an important consideration. Even simple analytical tools can help identify potential risk items during conceptual and architectural design stages, while there is still time to influence device selection, mechanical design, post assembly calibration (electronic alignment), preliminary cost projections, and key schedule milestones. Taking this even further, others will find value in recognizing key MEMS IMU metrics and opportunities to replace triaxial inertial test equipment with natural motion available in their system to get to the best value (performance, total cost of deployment) out of their systems.



Mark Looney



Also by this Author:

[An Introduction to MEMS Vibration Monitoring](#)
[Volume 8, Number 2](#)

Mark Looney [mark.looney@analog.com] is an *iSensor*® applications engineer at Analog Devices in Greensboro, North Carolina. Since joining ADI in 1998, he has accumulated experience in sensor-signal processing, highspeed analog-to-digital converters, and dc-to-dc power conversion. He earned a B.S. (1994) and M.S. (1995) degree in electrical engineering from the University of Nevada, Reno, and has published several articles. Prior to joining ADI, he helped start IMATS, a vehicle electronics and traffic solutions company, and worked as a design engineer for Interpoint Corporation.